Progress In Electromagnetics Research, Vol. 145, 195–202, 2014

Performance of an Implanted Electrically Coupled Loop Antenna inside Human Body

Ali Ibraheem and Majid Manteghi*

Abstract—Implanted antennas are widely used in hyperthermia and biomedical applications. The antenna needs to be extremely small while maintaining a permissible Specific Absorption Rate (SAR) and being able to cope with the detuning effects due to the dielectric properties of human body tissues. Most of the proposed antennas for implanted applications are electric field antennas such as Planner Inverted-F Antennas (PIFA) and micro-strip patch antennas. By minimizing the size of an electric field antenna, the near zone electric field will increase, resulting in higher SAR. This work is devoted to design a miniaturized magnetic field antenna to overcome the above limitations. The proposed electrically coupled loop antenna (ECLA) has high magnetic field and low electric field in the near zone and therefore, has a small SAR and is less sensitive to detuning effects. ECLA is designed at the Medical Implanted Communication Service (MICS) band with dimensions of ($5 \times 5 \times 3\,\mathrm{mm}^3$). ECLA has been simulated inside one-layer human body model, three-layer spherical human head model, human head and human body. From the simulation results, ECLA inside the human body has a 5 MHz–3 dB bandwidth, -14 dB gain, and radiation efficiency of 0.525%. The 1 g average SAR inside the human body for 10 mW input power is about 1 W/kg which is 7 times lower than the SAR for a patch antenna of the same size with the same accepted power.

1. INTRODUCTION

Implanted antennas inside human or animal bodies are widely used in biomedical telemetry (biotelemetry) and therapy applications. In biotelemetry, the implanted antennas are used to transmit into or out of the host body while in therapy applications, the implanted antennas are used to provide energy as cancer treatment using hyperthermia applications [1].

The common frequency bands for implanted antennas, approved by United States Federal Communication Commissions (FCC) and European communication Commissions (ERC), are Medical Implanted Communication Service (MICS) band (402–405 MHz) and Industrial Scientific and Medical (ISM) band (2.4–2.5 GHz). The choice of the frequency band decides the implanted antenna size and power loss inside the host body. The antennas operating at the MICS band have lower loss and larger antenna size, while on the other hand, the ISM band devices use smaller antennas having higher loss [2].

The design of an implanted antenna involves many challenges including biocompatibility, miniaturization, detuning effects of human body tissues, and patient safety. The implanted antenna must be biocompatible to prevent a short circuit which can occur due to the high conductivity of the human body tissues and to prevent rejection of the implanted antenna by the host body. To achieve biocompatibility, the implanted antenna should be surrounded by a biocompatible insulation layer such as PEEK, MACRO or Ceramic alumina. The dielectric properties of the human body tissues can change the resonant frequency of the implanted antenna. Therefore, the implanted antenna should be as robust

Received 20 February 2014, Accepted 16 March 2014, Scheduled 24 March 2014

* Corresponding author: Majid Manteghi (manteghi@vt.edu).

The authors are with the Bradley Department of Electrical and Computer Engineering, Virginia Polytechnic Institute and State University, VA 24061, USA.

as possible versus detuning effects. The antenna size has to be extremely miniaturized to satisfy the implanted devices requirements at the MICS band where the wavelength is about 750 mm. For the patient's safety, the power loss inside human body, which is measured by the Specific Absorption Rate (SAR), should be minimized. According to the FCC and ERC, the maximum limits for SAR averaged over 1 g and 10 g of tissue mass is 1.6 and 2 W/kg respectively [3, 4].

The early generations of implanted devices which use inductive coupling for communications, were able to transmit data over only a 2 cm range [5]. Most of the previous investigations on implanted antenna designs such as: micro-strip and Planar Inverted-F Antenna (PIFA) [6–11], cavity slot antenna [12–15] and dipole or monopole antennas [16–18] suffer from two main problems: high value of SAR at small antenna size and detuning effects due to the dielectric properties of the human body tissues. An electrically coupled loop antenna (ECLA) is proposed in this paper to tackle all the above issues.

The paper is organized as follows, the structure of ECLA will be described in Section 2 and the performance of ECLA in different human body models will be simulated in Section 3. In Sections 4 and 5, the effects of human model dimensions and the insulation layer on the value of the antenna's SAR will be investigated respectively. In Section 6, we make a few observations and conclude the paper.

2. ECLA STRUCTURE

Electrically Coupled Loop Antenna (ECLA), has been introduced previously [19] as a magnetic field antenna. It consists of a high impedance transmission line, i.e., inductor, terminated to a short circuit at one end and a distributed capacitor at the other end providing a distributed LC resonator. The feeding probe is electrically coupled to the antenna as well (Figure 1). The antenna can be tuned to a particular frequency using the antenna dimensions (L, W, and h) and the distributed capacitance between the loop and the ground plane (t_s, W_s and L_s). The dimensions of the feeding head (L_p, W_p and t_p) are responsible for scaling the input impedance of the antenna allowing us to match it to different impedances. ECLA can be extremely miniaturized by adding a lumped capacitor in parallel to the distributed capacitor of the resonant antenna. One can employ a variable capacitor to use the ECLA as a tunable antenna as well.

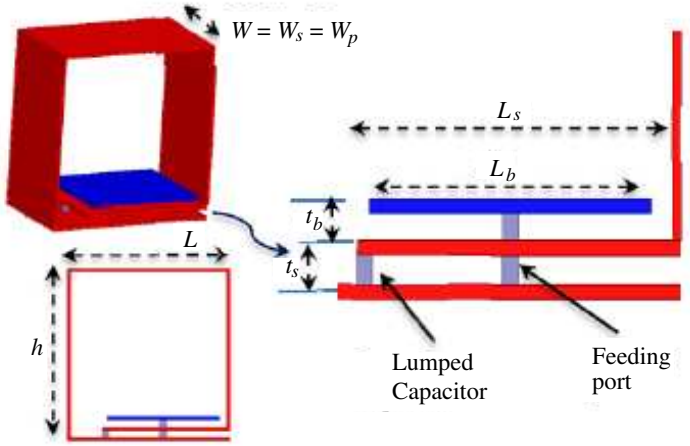

Figure 1. ECLA structure: front view and magnified view of feeding head and capacitance section.

3. ECLA PERFORMANCE INSIDE HUMAN BODY

The dimensions of ECLA (L, W, and h) used for the simulation in this section are ($5 \times 5 \times 3\,\text{mm}^3$), respectively. A shunt capacitor of 29 pF has been added in parallel with the distributed capacitor to reduce the resonant frequency of the antenna to 403.5 MHz. In the following subsections, the performance of the antenna will be studied inside different models of the human body.

3.1. One-Layer Model

To study the performance and radiation characteristics of ECLA inside human body, first a one-layer model is considered. One-layer model reduces the size of the numerical model and allows us to optimize the antenna using HFSS (Figure 2) in a reasonable time. Different tissues have been used for the one-layer model (Table 1) [6]. The one-layer model is a $100 \times 100 \times 100\,\text{mm}^3$ cube and ECLA is located at the center of the model. To achieve compatibility between the ECLA and the human body tissues, ECLA is covered by a 1 mm-thick insulation layer (whose effects will be discussed in Section 5). The scattering parameter (S_{11}) of ECLA inside skin and muscle tissues are presented in Figure 3. Based on this figure, one can conclude that the input impedance of ECLA does not vary dramatically by changing the electrical properties of the surrounding materials. Table 2 shows the radiation characteristics (maximum gain, -3 dB bandwidth, efficiency and 1 g averaged SAR inside the model) of ECLA compared to the previous work of implanted antennas [3]. This table shows that ECLA has the smallest size while still maintaining the lowest value of SAR.

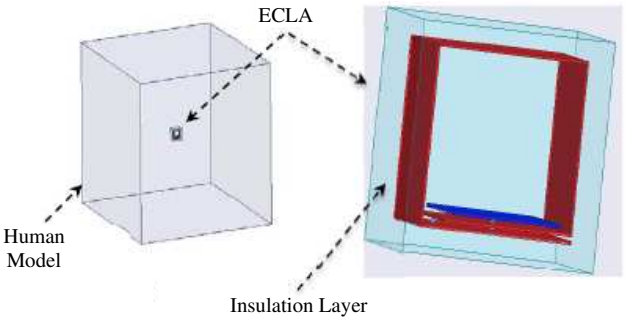

Figure 2. ECLA inside one-layer model of human body and magnified ECLA antenna structure.

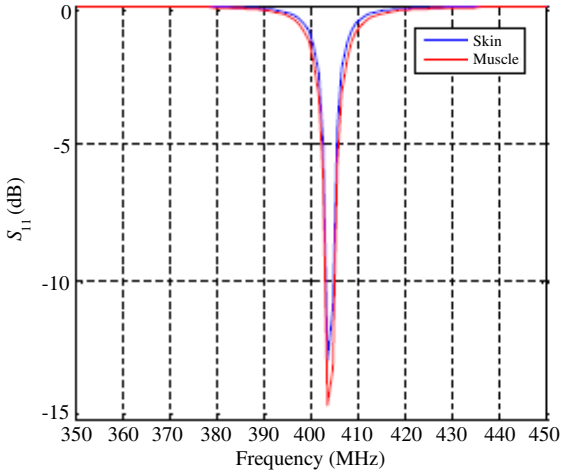

Figure 3. Scattering parameter of ECLA inside one-layer model for skin and muscle tissues.

Table 1. Dielectric properties of human body tissues.

Tissue	Dielectric constant	Conductivity (S/m)	Density (kg/m^3)
Skin	47.6	0.68	1100
Muscle	53.8	1.18	1040
Fat	5.57	0.041	1000
Skull	17.8	0.16	1850
Brain	49.7	0.59	1030

3.2. Three-layer Spherical Model

The next step would be simulating the optimized antenna in a three-layer model (Figure 4). Three-layer model is a more accurate model for the human head. The model consists of a brain layer with a radius of 85 mm and skull and skin layers with thickness of 10 and 5 mm respectively. ECLA is placed at the center of the three-layer model and simulated using HFSS. The scattering parameter (S_{11}) of ECLA inside the three-layer model is compared to those inside one-layer models of skin and muscle in Figure 5. This figure shows that the scattering parameter of the antenna is the same for all three-models.

Table 2. Radiation characteristics of ECLA compared to other types of implanted antennas.

Antenna Dimensions (mm)	Gain (dB)	Bandwidth (MHz)	Efficiency (%)	SAR (W/kg)
PIFA $(10 \times 10 \times 1.9)$	-26	50	0.6	336
PIFA $(8 \times 8 \times 1.9)$	-25	122	0.55	903
PIFA $(23 \times 19 \times 1.9)$	-27	120	$--$	280
Micro strip $(40 \times 32 \times 8)$	$--$	50	0.16	180
PIFA $(32 \times 24 \times 8)$	$--$	70	0.25	209
Spiral PIFA $(20 \times 24 \times 2.5)$	$--$	$--$	0.34	310
Stacked PIFA $(\pi \times 7.5 \times 1.9)$	-44	170	0.31	750
ECLA $(5 \times 5 \times 3)$	-14.7	5	0.4	152.8

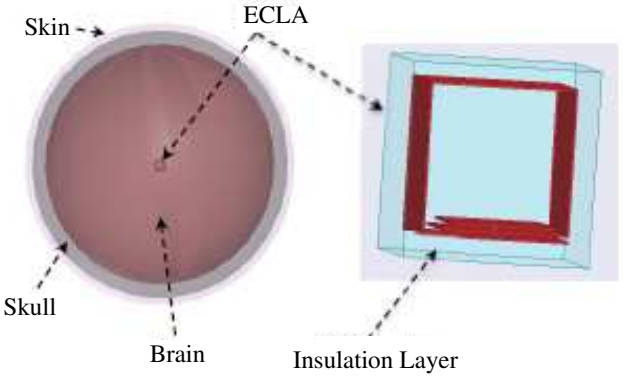

Figure 4. ECLA inside three-layer model of human head and magnified ECLA antenna structure.

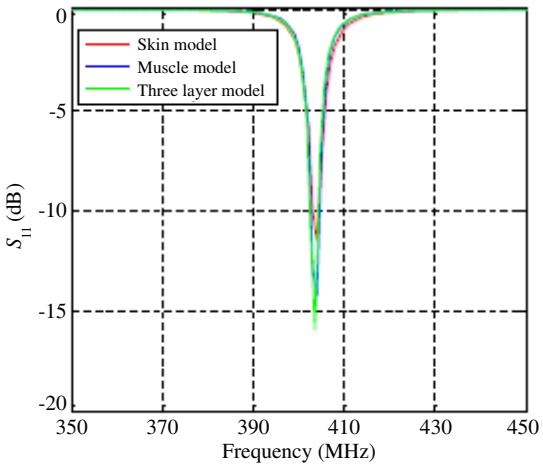

Figure 5. Scattering parameter of ECLA inside one-layer and three-layer models.

3.3. ECLA inside Human Head

To study the performance of ECLA inside human head, Remcom's XFDTD 7 (XF7) is employed with a model of human head consisting of 39 human tissues. ECLA is placed at the skin tissue (2 mm from skin surface) of the model as shown in Figure 6. The scattering parameter (S_{11}) of ECLA inside the human head model is shown in Figure 7. The antenna with dimensions ($5 \times 5 \times 3\,\text{mm}^3$) still has the same resonant frequency and a different value for the minimum scattering parameter. The antenna can be matched by changing the dimensions of the feeding probe. Also, 1 g-averaged SAR values of ECLA inside the head model are shown in Figure 8. The radiation characteristics of ECLA inside human head model are compared with the three-layer model in Table 3. From these results, one can conclude that the performance of ECLA inside the more accurate human head model is approximately the same as three-layer model.

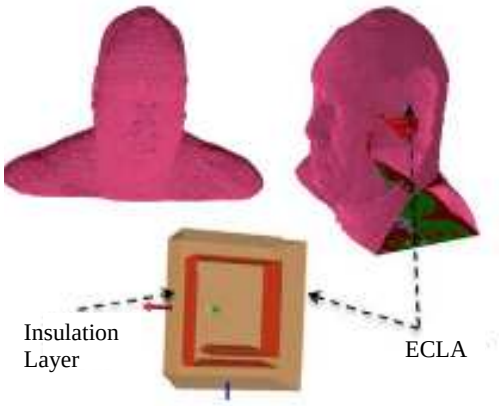

Figure 6. ECLA antenna inside human head and cutting plane to show ECLA antenna.

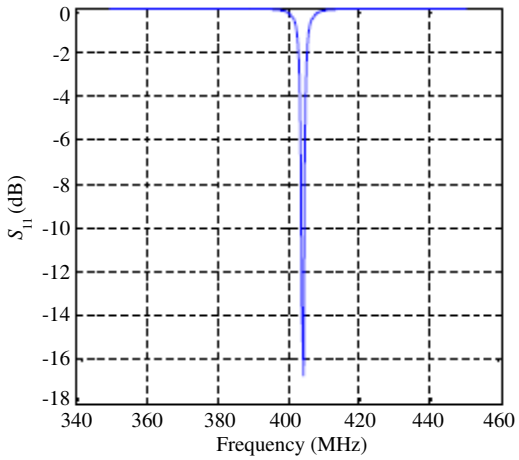

Figure 7. Scattering parameter of ECLA inside human head model.

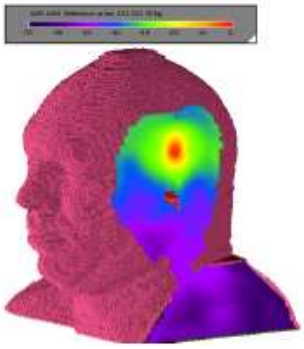

Figure 8. 1 g-averaged SAR of ECLA inside human head.

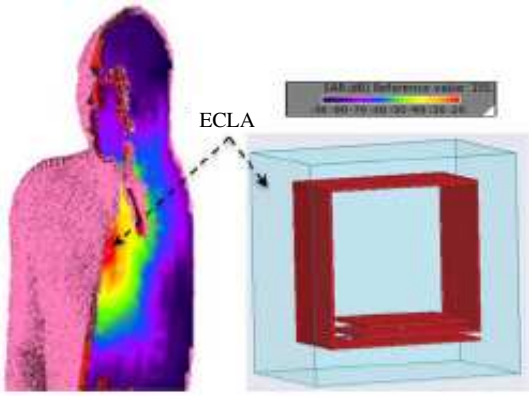

Figure 9. ECLA inside human body, cutting plane to show ECLA structure and its 1 g-averaged SAR inside human body.

Table 3. Radiation characteristics of ECLA inside three-layer spherical model and exact head.

Model	Gain (dB)	Bandwidth (MHz)	Efficiency (%)	SAR (W/kg)
Three-layer	−14.9	5	0.4	152
Head	−15	6	0.3	151

3.4. ECLA inside Human Body

The radiation characteristics of ECLA are investigated inside a human body using XF7 software as well. The model includes 39 human body tissues of an adult male. ECLA is placed at the shoulder of human body model as shown in Figure 9. The simulation results for the scattering parameter (S_{11}) of ECLA inside human body model are shown in Figure 10. This figure confirms that the impedance characteristics of ECLA do not change dramatically due to environmental effects.

4. EFFECT OF ECLA DIMENSIONS ON SAR

The dimensions of any implanted antenna have an important effect in its performance inside the human body. Specifically, the miniaturization factor has a significant role in deciding the SAR value. Table 4

Table 4. Radiation characteristics of ECLA inside one layer model with different ECLA dimensions.

ECLA dimensions (mm)	Quality factor (Q)	Bandwidth (MHz)	SAR1 g (W/kg)	SAR10 g (W/kg)
$5 \times 5 \times 3$	50	8	154	44
$6 \times 6 \times 4$	37	11	151	40
$7 \times 7 \times 5$	29	14	143	39
$8 \times 8 \times 6$	25	17	138	38
$9 \times 9 \times 7$	20	20	125	36
$10 \times 10 \times 8$	18	23	115	32

shows the effect of ECLA dimensions on its performance while maintaining the same resonant frequency by using different values of the lumped capacitor. The field intensity around the antenna increases by $1/a^p$ where a is the maximum dimension of the antenna and p is larger than 1 for an antenna size $a < \lambda/4$ [20]. This causes a significant jump in the SAR value for highly miniaturized electric field antennas. Due to the fact that ECLA is a magnetic antenna, the miniaturization factor does not increase the SAR dramatically compared to an electric antenna with the same size (Table 2).

5. EFFECT OF INSULATION LAYER ON SAR

To prevent the rejection of the implanted antenna by the human body tissues, ECLA with dimensions ($5 \times 5 \times 3\,\text{mm}^3$) is surrounded by a biocompatible insulation layer. The insulation layer thickness and type play an important role on the SAR of ECLA inside the human body model. Tables 5 and 6 show the performance of ECLA surrounded by different types of insulations with different thickness inside one-layer model of the human body. The radiation characteristics of ECLA are calculated using HFSS software.

Table 5. Radiation characteristics of ECLA inside one layer human body model with different PEEK material insulation thickness.

Insulation thickness (mm)	Gain (dB)	Bandwidth (MHz)	Efficiency (%)	SAR1 g (W/kg)
1	−15.5	8	0.35	154
2	−14.8	7.2	0.38	74.9
3	−14.5	6.9	0.42	41.2
4	−14.4	6.6	0.43	25.2
5	−14.2	6.4	0.45	15.7
6	−14.1	6.2	0.46	11

Table 6. Radiation characteristics of ECLA inside on layer human body model with different insulation materials.

Insulation Types	Gain (dB)	Bandwidth (MHz)	Efficiency (%)	SAR1 g (W/kg)
Teflon	−14.7	5	0.4	152.8
MACRO	−15.5	6	0.35	141.4
PEEK	−15.3	9	0.34	173.5
Ceramic Alumina	−16	11.2	0.28	201

It can be seen from the results presented in Tables 5 and 6 that the size and type of the insulating material can change the performance of the implanted ECLA. The capacitive part of the antenna (distributed capacitor) has the highest electric field intensity compared to the inductive parts [19].

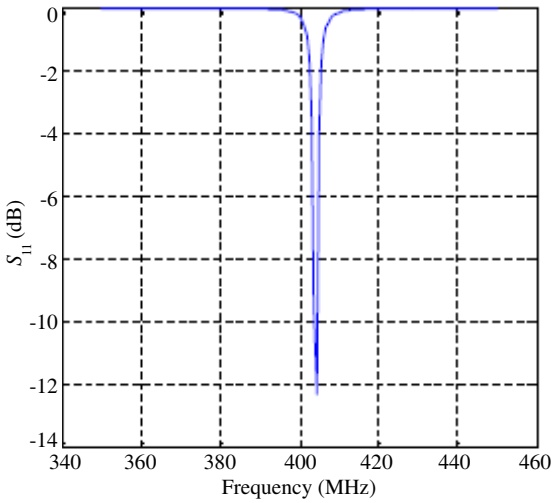

Figure 10. Scattering parameter of ECLA inside human body.

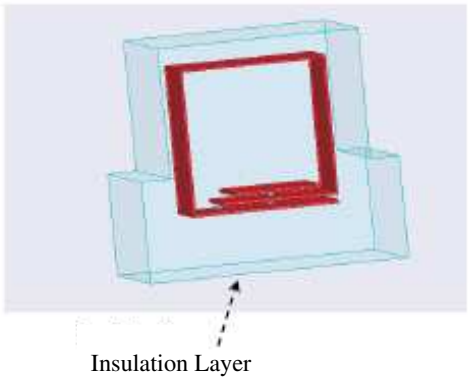

Figure 11. ECLA surrounded with insulation layer around the feeding head.

Table 7. The ECLA performance with different insulation thickness around feeding head and capacitance.

ECLA Volume (mm^3)	Gain (dB)	Bandwidth (MHz)	Efficiency (%)	SAR1 g (W/kg)
337	−18.3	4.2	0.17	48
252.3	−18.5	4.1	0.17	71
168.2	−28.4	3.7	0.17	81.6
121	−18.7	3.9	0.16	113

Since the electric field intensity is responsible for increasing the SAR values, one needs to either make the distributed capacitor smaller or use thicker insulating material layer around it (Figure 11). The performance of ECLA has been computed using HFSS inside one-layer human body model with different size of insulating material layer around the feeding probe and the results are presented in Table 7.

The inductive part of the antenna has the same size insulating material while the thickness of the insulating layer increases at capacitive part. The results presented in Table 7 when compared to the results obtained in Table 3 demonstrate the effectiveness of this method.

6. CONCLUSION

The electrically coupled loop antenna, ECLA, was proposed as a suitable candidate for an implanted antenna. Different parameters of the antenna were studied for various cases to demonstrate the effectiveness of ECLA for implanted devices. The simulation results showed that while ECLA has the smallest size among the published results in the literature, it maintains the smallest value of averaged SAR inside different types of human body models. Also, ECLA was shown to be insensitive to detuning effect due to dielectric properties of human body tissues. The effect of insulating material around ECLA was studied as well. It was shown that a thicker layer of insulation around the distributed capacitor can reduce the SAR.

REFERENCES

1. Patel, M. and J. Wang, "Applications, challenges, and prospective in emerging body area networking technologies," *IEEE Wireless Communications*, Vol. 17, 80–88, 2010.

2. Merli, F., L. Bolomey, J. Zurcher, G. Corradini, E. Meurville, and A. K. Skriverviky, "Design, realization and measurements of a miniature antenna for implantable wireless communication systems," *IEEE Transactions on Antennas and Propagation*, Vol. 59, 3544–3555, 2011.
3. Kiourti, A. and K. S. Nikita, "A review of implantable patch antennas for biomedical telemetry: Challenges and solutions [wireless corner]," *IEEE Antennas and Propagation Magazine*, Vol. 54, 210–228, 2012.
4. Karlsson, A., "Physical limitations of antennas in a lossy medium," *IEEE Transactions on Antennas and Propagation*, Vol. 52, 2027–2033, 2004.
5. Hall, P. S. and Y. Hao, "Antennas and propagation for body centric communications," *First European Conference on Antennas and Propagation 2006, EuCAP 2006*, 1–7, 2006.
6. Jaehoon, K. and Y. Rahmat-Samii, "Implanted antennas inside a human body: Simulations, designs, and characterizations," *IEEE Transactions on Microwave Theory and Techniques*, Vol. 52, 1934–1943, 2004.
7. Soontornpipit, P., C. M. Furse, and C. You Chung, "Design of implantable microstrip antenna for communication with medical implants," *IEEE Transactions on Microwave Theory and Techniques*, Vol. 52, 1944–1951, 2004.
8. Lee, C. M., T. C. Yo, C. H. Luo, C. H. Tu, and Y. Z. Juang, "Compact broadband stacked implantable antenna for biotelemetry with medical devices," *Electronics Letters*, Vol. 43, 660–662, 2007.
9. Lee, C. M., T. C. Yo, F. J. Huang, and C. H. Luo, "Dual-resonant π-shape with double L-strips PIFA for implantable biotelemetry," *Electronics Letters*, Vol. 44, 837–838, 2008.
10. Azad, M. Z. and M. Ali, "A miniature implanted inverted-F antenna for GPS application," *IEEE Transactions on Antennas and Propagation*, Vol. 57, 1854–1858, 2009.
11. Namjun, C., T. Roh, J. Bae, and H. J. Yoo, "A planar MICS band antenna combined with a body channel communication electrode for body sensor network," *IEEE Transactions on Microwave Theory and Techniques*, Vol. 57, 2515–2522, 2009.
12. Sze, J. Y., J. C. Wang, and C. C. Chang, "Axial-ratio bandwidth enhancement of asymmetric-CPW-fed circularly-polarised square slot antenna," *Electronics Letters*, Vol. 44, 1048–1049, 2008.
13. Wei, X., K. Saito, M. Takahashi, and K. Ito, "Performances of an implanted cavity slot antenna embedded in the human arm," *IEEE Transactions on Antennas and Propagation*, Vol. 57, 894–899, 2009.
14. Sze, J.-Y., C. I. G. Hsu, Z.-W. Chen, and C.-C. Chang, "Broadband CPW-fed circularly polarized square slot antenna with lightening-shaped feedline and inverted-L grounded strips," *IEEE Transactions on Antennas and Propagation*, Vol. 58, 973–977, 2010.
15. Pan, S. P., J. Y. Sze, and P.-J. Tu, "Circularly polarized square slot antenna with a largely enhanced axial-ratio bandwidth," *IEEE Antennas and Wireless Propagation Letters*, Vol. 11, 969–972, 2012.
16. Jones, K. M., J. A. Mechling, J. W. Strohbehn, and B. S. Trembly, "Theoretical and experimental SAR distributions for interstitial dipole antenna arrays used in hyperthermia," *IEEE Transactions on Microwave Theory and Techniques*, Vol. 37, 1200–1209, 1989.
17. Gosalia, K., M. S. Humayun, and G. Lazzi, "Impedance matching and implementation of planar space-filling dipoles as intraocular implanted antennas in a retinal prosthesis," *IEEE Transactions on Antennas and Propagation*, Vol. 53, 2365–2373, 2005.
18. Lin, H.-Y., M. Takahashi, K. Saito, and K. Ito, "Performance of implantable folded dipole antenna for in-body wireless communication," *IEEE Transactions on Antennas and Propagation*, Vol. 61, 1363–1370, 2013.
19. Manteghi, M., "Electrically coupled loop antenna as a dual for the planar inverted-F antenna," *Microwave and Optical Technology Letters*, Vol. 55, 1409–1412, 2013.
20. Kim, O. S., "Minimum Q electrically small antennas," *IEEE Transactions on Antennas and Propagation*, Vol. 60, 3551–3558, 2012.